European Radiology (2018) 28:4306–4313
https://doi.org/10.1007/s00330-018-5442-y

HEAD AND NECK

Diagnostic value of six MRI features for central neurocytoma

Xiaodan Li[1] · Liuji Guo[1] · Sen Sheng[2] · Yikai Xu[1] · Lichao Ma[1] · Xiang Xiao[1] · Zhiguang Si[1,3] · Yanping Chen[1] · Yuankui Wu[1]

Received: 1 January 2018 / Revised: 1 March 2018 / Accepted: 20 March 2018 / Published online: 30 April 2018

Abstract

Objectives To increase our understanding of the imaging features of central neurocytoma (CN) and improve the preoperative MRI diagnosis accuracy.

Methods Preoperative MR images of 30 CNs and another 68 intraventricular non-CN tumours were analysed by one experienced neuroradiologist retrospectively to identify previously reported features and new features of CN. Six blinded radiologists independently reviewed all these MRI images, and scored all characteristic features on a five-point scale. Diagnostic value was assessed by the area under the receiver operating characteristic curve (AUC); sensitivity, specificity and accuracy were also calculated.

Results In addition to the 'scalloping' sign, 'broad-based attachment' sign and 'soap-bubble' sign, three new MRI features of CN were identified, including the 'peripheral cysts' sign, 'fluid-fluid level' sign and the 'gemstone' sign. The scalloping sign showed the highest AUC value (0.82), followed by the peripheral cysts sign (0.75) and broad-based attachment sign (0.75). The scalloping sign exhibited the highest specificity (82%), followed by the fluid-fluid level sign (79%) and gemstone (78%) sign. The broad-based attachment sign (85%) was the most sensitive feature, followed by the soap-bubble sign (84%) and peripheral cysts sign (77%).

Conclusion There are six characteristic MRI features that help to improve the preoperative diagnostic accuracy of CN.

Key Points

- *This study is the largest magnetic resonance imaging (MRI) cohort on central neurocytoma (CN).*
- *Three new features helpful for the diagnosis of CN were reported.*
- *Diagnostic value of six MRI features of CN was preliminarily determined.*

Keywords Cerebral ventricle neoplasms · Neurocytoma · Magnetic resonance imaging · Diagnostic imaging · ROC curve

Abbreviations

AUC	Area under the curve
CN	Central neurocytoma
ROC	Receiver operating characteristic
SE	Standard error

Xiaodan Li and Liuji Guo contributed equally to this study and are considered co-first authors

✉ Yuankui Wu
ripleyor@126.com

[1] Department of Medical Imaging, Nanfang Hospital, Southern Medical University, No. 1838 Guangzhou Avenue North, Guangzhou, China

[2] Neurology Department, University of Arkansas for Medical Science, Little Rock, AR, USA

[3] Department of Medical Imaging, People's Hospital of Dehong Prefecture, Yunnan, China

Introduction

Central neurocytoma (CN) was first described by Hassoun and his colleagues in 1982 [1] and was classified as a grade II neuronal and mixed neuronal-glial tumour [2]. Making up 0.25% to 0.5% of all intracranial tumours, CNs mostly occur in the lateral ventricles [3]. Patients with CN usually present with nonspecific symptoms caused by increased intracranial pressure and with nonspecific laboratory results [4, 5]. CN behaves like a benign lesion and is usually associated with a favourable prognosis following gross total surgical resection, which differs from other invasive tumours such as most astrocytomas, ependymomas and choroid plexus papillary carcinomas. Therefore, accurate preoperative diagnosis is vital for treatment planning for CNs [4, 6].

Magnetic resonance imaging (MRI) is the most widely used imaging modality for intracranial tumours. A few MRI features have been reported as being characteristic features for

CN, such as: (1) 'scalloping' sign: an appearance resembling a scallop and consisting of cysts on the periphery of the tumour and the wavy walls of the expanded lateral ventricle [7]; (2) 'broad-based attachment' sign: tumours have a broad-based attachment to either the septum pellucidum or walls of the lateral ventricle [5, 8, 9]; and (3)'soap-bubble' sign: also known as 'spongy' or 'cheese' appearance, representing clusters of cysts of various sizes displayed within the tumour [10–12]. However, there is not agreement on the value of these MRI features [4, 7], which calls for new specific MRI features for CNs, as well as the need to systematically analyse the diagnostic value of each feature in identifying CN.

The present study reported three new specific MRI features of CNs. Furthermore, we investigated the diagnostic value of all of these features through the receiver operating characteristic (ROC) curve analysis.

Materials and methods

Patients

This study was approved by the institutional review board. We used the picture archiving and communication system (PACS) program to search our radiology database retrospectively from January 2008 to May 2016 to obtain MRI data of CNs and other intraventricular tumours. 116 patients who underwent surgical treatment at our institution with routine preoperative MRI examination and whose postoperative pathological diagnosis confirmed by haematoxylin-eosin staining and immunohistochemistry were enrolled into this study. Eighteen cases (two cases of CNs, seven meningiomas, one choroid plexus papillary tumour, four ependymal tumours and four astrocytomas) were excluded for motion artifacts (six cases) or for incomplete or unavailable MRI data (12 cases). Eventually, 98 cases of intraventricular tumours were included in this study, including 30 cases of CNs, 18 meningiomas, 10 choroid plexus papillary tumours, 18 ependymal tumours and 22 astrocytomas.

MRI parameters

Patients were examined on 3.0T MRI scanners (including GE Signa Excite 3.0T and Philips Achieva 3.0T) with the use of a head or head-neck coil. All of the 98 patients underwent MRI protocols comprised of axial T1WI (TE 14–23.7 ms, TR 400–754 ms), T2WI (TE 76–138 ms, TR 3,000–5,100 ms) and axial, sagittal and coronal contrast-enhanced T1WI (TE 4.6–23.4 ms, TR 189–750 ms). Axial fluid-attenuated inversion recovery (FLAIR) sequence was performed in 64 patients. For all patients, contrast agent (Omniscan TM, GE Healthcare, Ireland; Magnevist, Schering, Berlin, Germany; gadopentetate dimeglumine, Consun, Guangzhou, China) was administered at a dose of 0.2 mmol/kg and a rate of 2.0–2.5ml/s, using a power injector (Spectris Solarisl EP, Medrad, USA; TennesseeXD003, Ulrich Medical, Germany) through the antecubital vein, followed by a 20-ml sterile saline flush. Matrices of the sequences were from 480 × 480 to 512 × 512.

Image analysis

One radiologist (YK W, with 15 years of experience in neurology imaging) observed all MR images carefully to identify the scalloping sign, broad-based attachment sign and soap-bubble sign, and searched for new features and formulated the definitions for them all (see Results section).

All of these features and their definitions were introduced to six radiologists (LC M, LJ G and X X, with 5 years of experience; ZG S with 10 years of experience; YP C and YK X with 25 years of experience). The radiologists, blinded to histopathological diagnoses, independently recorded the confidence level of the presence of every single feature in each case of intraventricular tumour using a 5-point scale: 1 = definitely not present; 2 = probably not present; 3 = equivocal; 4 = probably present; 5 = definitely present. The window width, window level and zoom of images were adjusted through the tools included in the PACS program as needed.

Statistical analysis

Kendall's coefficient of concordance W was used to determine inter-rater agreement, with W ≥.21 representing fair, W ≥.41 moderate, W ≥.61 substantial and W ≥.81 almost perfect concordances. ROC curve analysis was performed to assess the diagnostic performance using SPSS 19.0 software, with CN cases scored as 1, while non-CN cases were marked as 0 according to the gold standard served by pathological diagnosis. Areas under the curves (AUCs), sensitivities, specificities and accuracies of each MRI feature were calculated. The comparison between every two AUCs was tested by the two-tailed Z-test of Delong & Clarke-Pearson conducted in MedCalc (Version 11.4.2.0) software. False discovery rate (FDR) control was used to correct for multiple comparisons. The difference was considered statistically significant if $p<0.05$.

Results

MRI features of CN

Scalloping sign, broad-based attachment sign and soap-bubble sign were noted in the CNs enrolled in the present study (Figs. 1a–f, 2a–c). Additionally, three new characteristic MRI features of CN were found and defined: (1) 'peripheral

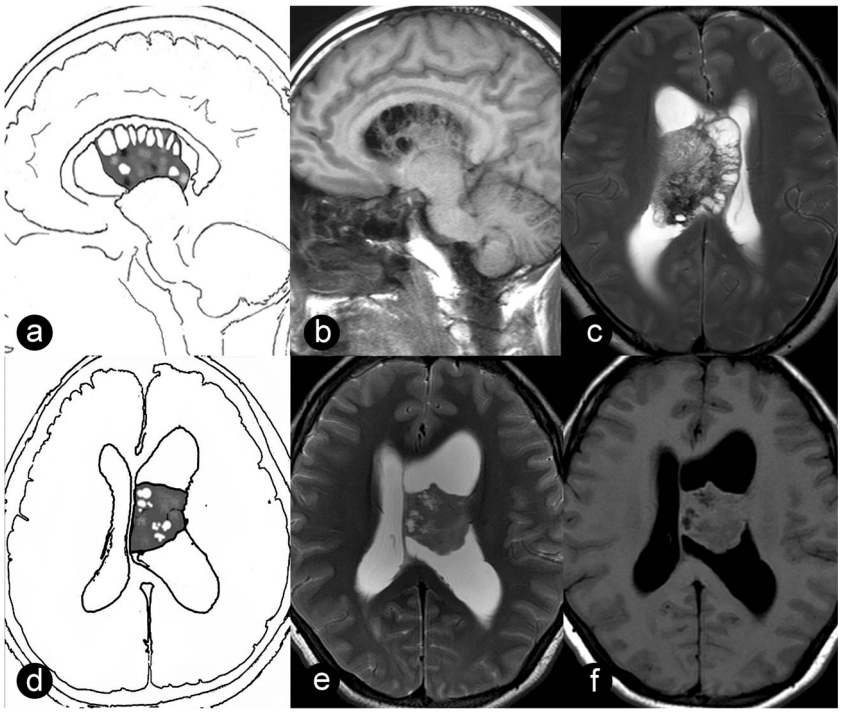

Fig. 1 Scalloping sign and broad-based attachment sign. (**a**) Sample graph, (**b**) sagittal T1WI and (**c**) axial T2WI of scalloping sign: the radial lines – formed by the walls of numerous cysts along the borders of the mass, and the undulate wall of the lateral ventricular make up a picture similar to that of a scallop. (**d**) Sample graph, (**e**) axial T2WI and (**f**) axial T1WI of broad-based attachment sign: the mass abuts the septum pellucidum with a broad base

cyst' sign (Fig. 2d–f): multiple cysts located at the periphery of the mass, with or without the presence of central cysts; (2) 'fluid-fluid level' sign (Fig. 3a–c), an interface between the upper (usually hyper-intense on T2WI) and lower (commonly hypo-intense or iso-intense on T2WI) parts of tumour cysts; and (3) 'gemstone' sign (Fig. 3d–f), which was shown on contrast-enhanced T1-weighted images as single or multiple well-defined small foci of strong enhancement, in contrast to the negligible enhancement of the majority of tumours. Several representative cases of the MRI features, which contributed greatly to the accurate differential diagnosis between CN and non-CN, are shown in Figs. 4 and 5.

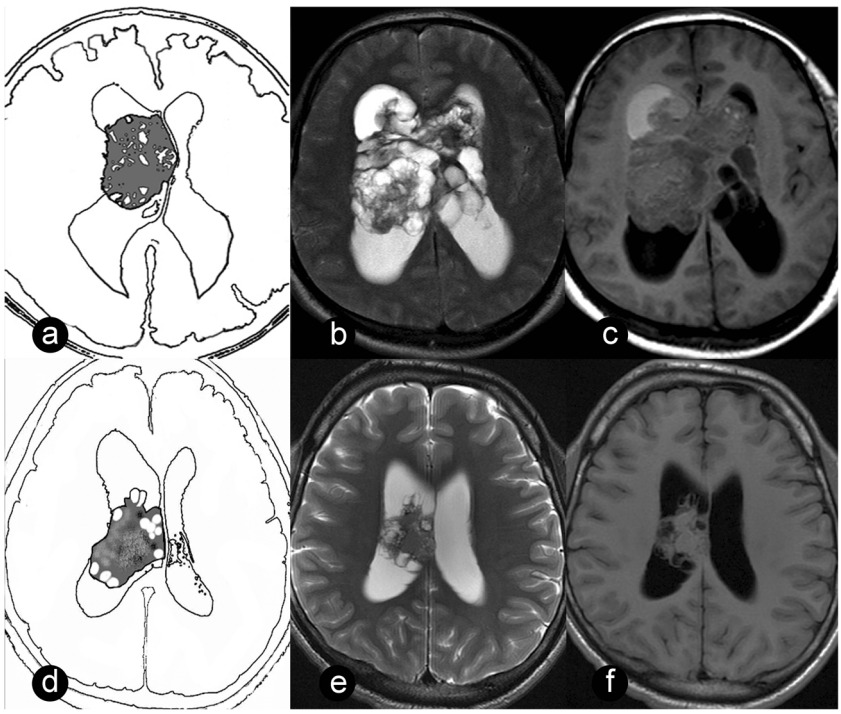

Fig. 2 Soap-bubble sign and peripheral cysts sign. (**a**) Sample graph, (**b**) axial T2WI and (**c**) axial T1WI of soap-bubble sign: a large number of cysts varying in sizes within the mass form the pattern resembling soap bubbles or sponge. (**d**) Sample graph, (**e**) axial T2WI and (**f**) axial T1WI of peripheral cysts sign: a few cysts are scattered along the periphery of the mass

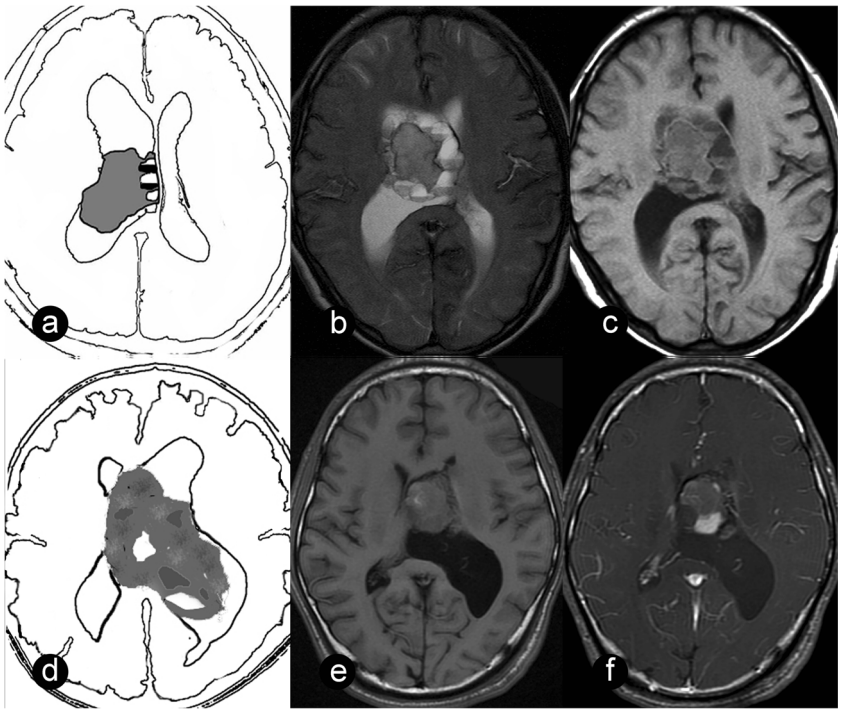

Fig. 3 Fluid-fluid level sign and gemstone sign. (**a**) Sample graph, (**b**) axial T2WI and (**c**) axial T1WI of fluid-fluid level sign: the fluid-fluid interface divided each cyst inside the mass into two parts with different signal intensity. (**d**) Sample graph, (**e**) pre-contrast and (**f**) post-contrast axial T1WI of gemstone sign: single area of strong enhancement with distinct border was shown on the mildly enhanced tumour background

Inter-rater agreement for each MRI feature

Table 1 summarizes the W values of six MRI features. The peripheral cysts sign ranked the highest inter-rater concordance (0.76), with the same level of concordance (substantial) as the scalloping sign, soap-bubble sign and broad-based attachment sign. A moderate inter-rater agreement was recorded for the gemstone sign and fluid-fluid level sign.

Diagnostic performance of six features of CN

The AUC values of the six features were all above 0.5, with the scalloping sign being the highest (0.82), followed by the peripheral cysts sign (0.75) and broad-based attachment sign (0.75) (Fig. 6, Table 2, Z-test result is shown in Table 3; the results of all ratings is shown in Table 4). The scalloping sign also presented the maximum specificity (82%). Fluid-fluid level sign, gemstone sign and peripheral cysts sign showed

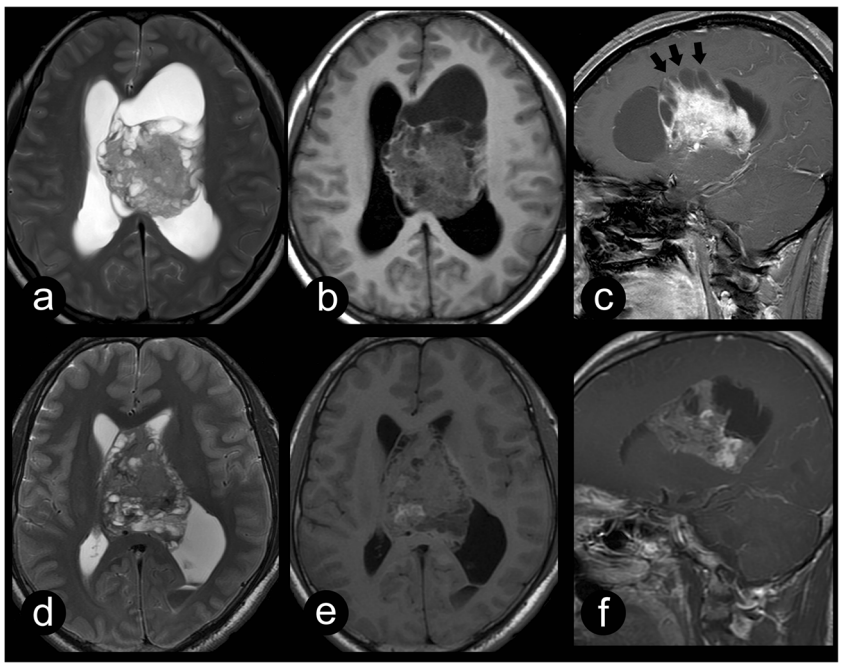

Fig. 4 Differentiation between central neurocytoma (CN) and ependymoma with scalloping sign. **Upper row**: female, 33 years old, CN; **lower row**: male, 28 years old, ependymoma. Axial T2WI (**a**, **d**) and T1WI (**b**, **e**) of both cases show multiple cysts in the mass (**d**); on post-contrast sagittal T1WI (**c**, **f**), CN showed the peripheral cysts between the mass and the lateral ventricular wall (arrow), forming the scalloping sign, but ependymoma did not show the scalloping sign

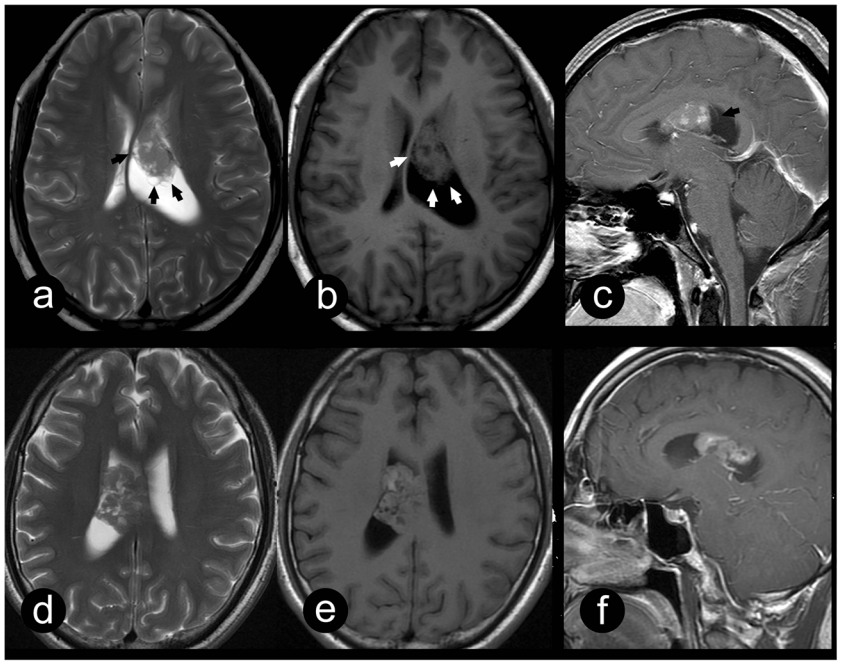

Fig. 5 Differentiation between central neurocytoma (CN) and astrocytoma with peripheral cysts sign. **Upper row**: male, 33 years old, CN; **lower row**: male, 42 years old, astrocytoma. Axial T2WI (**a**, **d**) and T1WI (**b**, **e**) revealed numerous cysts in both cases but with different patterns of distribution, mainly on its periphery in CN (arrow) and randomly in astrocytoma. On post-contrast sagittal T1WI (**c**, **f**), both masses showed heterogeneous enhancement and were attached to the roof of the ventricle with broad base

favourable specificities (≥70%). The broad-based attachment sign was the most sensitive feature (85%), followed by the soap-bubble sign (84%) and peripheral cysts sign (77%). The accuracy of the scalloping sign (80%) was significantly higher when compared to other signs (66%–72%).

Discussion

Despite its rarity, CN is an important differential diagnosis of intraventricular tumours [4, 12, 13]. The present study reported new MRI features of CN and evaluated all available characteristic MRI features, including the scalloping sign, broad-based attachment sign, soap-bubble sign, peripheral cysts sign, fluid-fluid level sign and gemstone sign, in terms of their ability to discriminate CN from non-CN patients.

There have been many reports on imaging manifestations of CN [1, 4, 5, 14, 15]. CNs mostly occur around the foramen of Monro in young people. On MRI, CN appears as commonly iso-intense on T1-weighted images (T1WI) and iso-intense or slightly hyper-intense on T2-weighted images (T2WI) relative to grey matter, and usually consists of cysts, calcifications and flow voids [5, 14, 15]. Obstructive hydrocephalus is usually present, but peritumoral oedema is rare [3, 10, 11]. However, it is challenging to distinguish CN from ependymal tumours and astrocytomas based on these general imaging findings [7, 16].

Table 1 Inter-rater agreement of six MRI features

Sign	Kendall's W	*p*-value
Peripheral cysts	0.76	<0.001
Scalloping	0.73	<0.001
Soap-bubble	0.63	<0.001
Broad-based attachment	0.61	<0.001
Gemstone	0.60	<0.001
Fluid-fluid level	0.53	<0.001

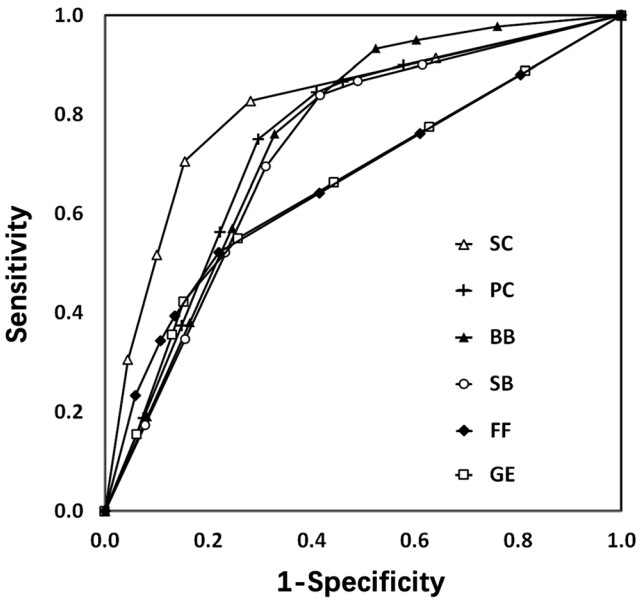

Fig. 6 Composite receiver operating characteristic (ROC) curves of six readers depict reader confidence in the diagnosis of central neurocytoma (CN) with the six characteristic MRI features. The scalloping sign showed the highest AUC (0.82) and specificity (82%). The peripheral cysts sign, broad-based attachment sign and soap-bubble sign exhibited similar AUC values, which were larger than those of the fluid-fluid level sign and gemstone sign. *SC* scalloping, *PC* peripheral cysts, *BB* broad-based attachment, *SB* soap-bubble, *FF* fluid-fluid level, *GE* gemstone

Table 2 AUC, sensitivity, specificity and accurracy of six MRI features for central neurocytomas (CNs)

Sign		Observer						Mean
		1	2	3	4	5	6	
SC	AUC	0.88	0.86	0.80	0.81	0.81	0.77	0.82
	Se	87%	83%	67%	80%	70%	70%	76%
	Sp	85%	82%	84%	71%	85%	82%	82%
	Ac	86%	82%	79%	74%	80%	78%	80%
PC	AUC	0.73	0.72	0.76	0.77	0.74	0.78	0.75
	Se	80%	83%	77%	70%	67%	87%	77%
	Sp	65%	58%	74%	77%	76%	70%	70%
	Ac	70%	66%	75%	75%	73%	75%	72%
BB	AUC	0.71	0.80	0.76	0.74	0.79	0.72	0.75
	Se	87%	83%	87%	87%	83%	83%	85%
	Sp	50%	71%	57%	57%	68%	57%	60%
	Ac	61%	75%	66%	66%	73%	65%	68%
SB	AUC	0.65	0.71	0.72	0.74	0.75	0.79	0.73
	Se	93%	90%	83%	83%	70%	87%	84%
	Sp	34%	51%	59%	62%	76%	68%	58%
	Ac	52%	63%	66%	68%	74%	74%	66%
FF	AUC	0.59	0.79	0.65	0.65	0.61	0.67	0.66
	Se	43%	77%	50%	47%	50%	47%	52%
	Sp	72%	82%	76%	87%	68%	87%	79%
	Ac	63%	80%	68%	75%	62%	75%	71%
GE	AUC	0.65	0.70	0.69	0.58	0.65	0.66	0.66
	Se	57%	67%	53%	37%	40%	60%	52%
	Sp	72%	69%	84%	82%	90%	74%	78%
	Ac	67%	68%	75%	68%	75%	70%	70%

SC scalloping, *PC* peripheral cysts, *BB* broad-based attachment, *SB* soap-bubble, *FF* fluid-fluid level, *GE* gemstone, *Se* sensitivity, *Sp* specificity, *Ac* accuracy

Table 3 Comparison of the AUC values for all feature pairs

Sign		SC	PC	BB	SB	FF	GE
SC	Z		3.197	2.845	4.442	6.580	5.891
	P		0.003	0.007	0.001	0.002	0.001
PC	Z	3.197		0.181	1.191	3.773	3.406
	P	0.003		0.856	0.292	0.001	0.002
BB	Z	2.845	0.181		1.111	3.579	3.487
	P	0.007	0.856		0.308	0.001	0.001
SB	Z	4.442	1.191	1.111		2.782	2.560
	P	0.001	0.292	0.308		0.008	0.014
FF	Z	6.580	3.773	3.579	2.782		0.200
	P	0.002	0.001	0.001	0.008		0.902
GE	Z	5.891	3.406	3.487	2.560	0.200	
	P	0.001	0.002	0.001	0.014	0.902	

SC scalloping, *PC* peripheral cysts, *BB* broad-based attachment, *SB* soap-bubble, *FF* fluid-fluid level, *GE* gemstone

Z-test results present as: Z value and *p* value after FDR control correction

Some MRI features were reported to improve the diagnostic accuracy of CNs [4, 5, 7–12]. The scalloping sign, originally described by a Japanese scholar, demonstrated higher accuracy than the soap-bubble sign to distinguish CNs from other types of intraventricular tumours [7]. In agreement with Niiro's point, it exhibited the best diagnostic performance among the six features included in our analysis. Moreover, this sign had the highest specificity. In addition, it showed great inter-rater agreement in our present study, which could decrease the doubt about its subjectivity [4]. However, its sensitivity was relatively low, which may be explained by the fact that it was typically depicted only in the sagittal view (Figs. 1b and 4c).

The broad-based attachment sign is closely associated with the site of origin of intraventricular tumours. CNs are derived from the small grey nuclei of the septum pellucidum or bipotential progenitor cells in the periventricular matrix [17–19]. Consequently, they lie alongside the septum pellucidum or the walls of the lateral ventricle with a broad base, especially on the superior wall of lateral ventricles. The broad-based attachment sign had the highest sensitivity in the present cohort. However, ependymal tumours and astrocytomas are also commonly found in these regions and tend to show the broad-based attachment sign. Thus, this feature demonstrated a high sensitivity but a low specificity for CN. Of note, CNs usually have conspicuous borders [20, 21], while ependymoma and astrocytoma grow aggressively and readily invade the parenchyma surrounding the ventricles. Therefore, it is important to observe further the clarity of tumour borders to differentiate CNs from ependymoma and astrocytoma, after identifying the broad-based attachment sign.

Up to 85% of CNs have numerous cysts [22], leading to the excellent sensitivity of the soap-bubble sign in the present study. However, its specificity was much lower than that of the periphery cyst sign, which may result from the lack of details and specifications about cysts' properties like spatial distribution, and from the high incidence of multiple cysts displayed in ependymal tumours and astrocytomas [11]. Cysts of most types of tumours are distributed centrally because this is the most common site of ischaemia and necrosis. However, in the present observation, cysts of CNs break this rule of thumb and tend to be found in the tumour's periphery. Therefore, we proposed the concept of the peripheral cysts sign, which was more specific to CN than the soap-bubble sign in this study (Fig. 5). Moreover, the peripheral cysts sign existed in every case with the scalloping sign and was visible from any view of MR images in this study, which may contribute to its greater sensitivity when compared with the scalloping sign. In addition, the peripheral cyst sign had the greatest inter-rater agreement. Based on the aforementioned results, peripheral cysts sign shows excellent clinical practicality. However, the pathological basis of this sign needs to be further understood.

Table 4 Summary of the scores given by six observers and AUCs of each MRI sign for the diagnosis of various tumours

Pathology	Sign	Score					AUC
		1	2	3	4	5	
Central neurocytoma (30)	SC	31[a]	22	34	38	55	0.82
	PC	18	6	4	17	135	0.75
	BB	4	5	3	31	137	0.75
	SB	18	6	5	26	125	0.73
	FF	86	23	9	20	42	0.66
	GE	81	23	12	36	28	0.66
Choroid plexus papillary tumours (10)	SC	57	2	0	1	0	0.55
	PC	31	6	3	7	13	0.58
	BB	18	15	5	11	11	0.59
	SB	32	10	4	0	14	0.59
	FF	53	5	1	1	0	0.56
	GE	56	3	0	1	0	0.52
Meningioma (18)	SC	102	4	2	0	0	0.55
	PC	80	10	3	5	10	0.58
	BB	52	27	9	13	7	0.59
	SB	72	8	8	9	11	0.59
	FF	103	3	1	1	0	0.56
	GE	93	5	2	7	1	0.52
Ependymal tumour (18)	SC	47	25	12	11	13	0.55
	PC	19	16	4	13	56	0.58
	BB	14	7	8	14	65	0.59
	SB	17	11	7	16	57	0.59
	FF	63	12	7	14	12	0.56
	GE	74	15	2	6	11	0.52
Astrocytoma (22)	SC	87	21	8	11	5	0.55
	PC	42	16	11	21	42	0.58
	BB	14	15	10	42	51	0.59
	SB	36	22	11	18	45	0.59
	FF	99	15	2	4	12	0.56
	GE	80	20	5	14	13	0.52

SC scalloping, *PC* peripheral cysts, *BB* broad-based attachment, *SB* soap-bubble, *FF* fluid-fluid level, *GE* gemstone

Numbers in brackets are the number of cases of each type of tumour. Numbers (a) listed in the table are frequencies of each score rated by six observers

The solid part of CNs display variable patterns of enhancement after contrast agent administration [4, 8, 9, 21], contributing little to the differentiation between CNs and non-CNs. After careful observation, we noticed one or several small strikingly enhanced areas with well-defined boundaries to the non-enhanced or mildly enhanced surroundings in CN on post-contrast T1WI images, which showed a high specificity for CNs. To the best of our knowledge, this feature has not been described previously, and, therefore, we named the sign 'gemstone' in the present study. The pathophysiological mechanism of this feature was unknown, which might be because of the unknown existence of capillaries with a peculiar structure [23] or some cavernous haemangioma-like changes.

The fluid-fluid level sign commonly results from haemorrhage [24]. Despite their rich vasculature, CNs bleed infrequently, which might in part lead to the lowest sensitivity of this feature presented in this report. Of note, the fluid-fluid level sign showed the lowest inter-rater agreement, which could be due to the tiny fluid-fluid level in small cysts and lead to its unsatisfactory sensitivity.

Our study has several limitations. We evaluated the diagnostic value of six individual characteristic features but not the value of these six features combined in any form or combined with general imaging features. Many other types of intraventricular tumours were not included in this study due to their rarity in our hospital, such as metastatic tumours, melanoma

and subependymal giant cell astrocytoma. In addition, no neurosurgeons participated in the study.

In conclusion, in this largest MRI cohort of CN to date, three new characteristic MRI features of CN were reported, i.e. 'peripheral cysts' sign, 'fluid-fluid level' sign and 'gemstone' sign. The combined six MRI features showed a practical and positive ability for CN diagnosis and differentiation, among which the scalloping sign allowed for the best performance and the peripheral cysts sign worked promisingly. A better understanding of these characteristic MRI features in the context of the age of onset and other general radiological findings may improve the diagnostic accuracy for CNs.

Funding This study has received funding by the Natural Science Foundation of Guangdong Province, China, the Science and Technology Program of Guangzhou, China, and the Special Foundation of President of Nanfang Hospital, Southern Medical University.

Compliance with ethical standards

Guarantor The scientific guarantor of this publication is Prof. Dr. Yuankui Wu, Department of Medical Imaging, Nanfang Hospital, Southern Medical University.

Conflict of interest The authors of this manuscript declare no relationships with any companies whose products or services may be related to the subject matter of the article.

Statistics and biometry No complex statistical methods were necessary for this paper.

Informed consent Written informed consent was waived by the Institutional Review Board.

Ethical approval Institutional Review Board approval was obtained.

Study subjects or cohorts overlap MRI data of 12 patients of CN have been previously reported in Journal of Neuro-Oncology.

Methodology
- retrospective
- diagnostic or prognostic study
- performed at one institution

References

1. Hassoun J, Gambarelli D, Grisoli F et al (1982) Central neurocytoma. An electron-microscopic study of two cases. Acta Neuropathol 2:151–156
2. Louis DN, Perry A, Reifenberger G et al (2016) The 2016 world health organization classification of tumors of the central nervous system: a summary. Acta Neuropathol 6:803–820
3. Koeller KK, Sandberg GD (2002) From the archives of the afip. Cerebral intraventricular neoplasms: radiologic-pathologic correlation. Radiographics 6:1473–1505
4. Donoho D, Zada G (2015) Imaging of central neurocytomas. Neurosurg Clin N Am 1:11–19
5. Chen CL, Shen CC, Wang J, Lu CH, Lee HT (2008) Central neurocytoma: a clinical, radiological and pathological study of nine cases. Clin Neurol Neurosurg 2:129–136
6. Kerkovsky M, Zitterbart K, Svoboda K et al (2008) Central neurocytoma: the neuroradiological perspective. Childs Nerv Syst 11:1361–1369
7. Niiro T, Tokimura H, Hanaya R et al (2012) Mri findings in patients with central neurocytomas with special reference to differential diagnosis from other ventricular tumours near the foramen of monro. J Clin Neurosci 5:681–686
8. Goergen SK, Gonzales MF, Mclean CA (1992) Interventricular neurocytoma: radiologic features and review of the literature. Radiology 3:787–792
9. Shin JH, Lee HK, Khang SK et al (2002) Neuronal tumors of the central nervous system: radiologic findings and pathologic correlation. Radiographics 5:1177–1189
10. Ramsahye H, He H, Feng X, Li S, Xiong J (2013) Central neurocytoma: radiological and clinico-pathological findings in 18 patients and one additional mrs case. J Neuroradiol 2:101–111
11. Smith AB, Smirniotopoulos JG, Horkanyne-Szakaly I (2013) From the radiologic pathology archives: intraventricular neoplasms: radiologic-pathologic correlation. Radiographics 1:21–43
12. Freund M, Jansen O, Geletneky K, Hahnel S, Sartor K (1998) Computerized tomography and magnetic resonance imaging findings in central neurocytoma. Rofo 5:502–507
13. Choudhari KA, Kaliaperumal C, Jain A et al (2009) Central neurocytoma: a multi-disciplinary review. Br J Neurosurg 6:585–595
14. Zhang D, Wen L, Henning TD et al (2006) Central neurocytoma: clinical, pathological and neuroradiological findings. Clin Radiol 4:348–357
15. Wang M, Jia D, Shen J, Zhang J, Li G (2013) Clinical and imaging features of central neurocytomas. J Clin Neurosci 5:679–685
16. Osztie E, Hanzely Z, Afra D (2009) Lateral ventricle gliomas and central neurocytomas in adults diagnosis and perspectives. Eur J Radiol 1:67–73
17. Jouvet A, Lellouch-Tubiana A, Boddaert N, Zerah M, Champier J, Fevre-Montange M (2005) Fourth ventricle neurocytoma with lipomatous and ependymal differentiation. Acta Neuropathol 3:346–351
18. Paek SH, Kim JE, Kim DG, Han MH, Jung HW (2003) Angiographic characteristics of central neurocytoma suggest the origin of tumor. J Korean Med Sci 4:573–580
19. von Deimling A, Kleihues P, Saremaslani P et al (1991) Histogenesis and differentiation potential of central neurocytomas. Lab Invest 4:585–591
20. Cheung YK (1996) Central neurocytoma occurring in the thalamus: ct and mri findings. Australas Radiol 2:182–184
21. Nishio S, Tashima T, Takeshita I, Fukui M (1988) Intraventricular neurocytoma: clinicopathological features of six cases. J Neurosurg 5:665–670
22. Chang KH, Han MH, Kim DG et al (1993) Mr appearance of central neurocytoma. Acta Radiol 5:520–526
23. Collins VP, Jones DT, Giannini C (2015) Pilocytic astrocytoma: pathology, molecular mechanisms and markers. Acta Neuropathol 6:775–788
24. Goel A, Shah A, Jhawar SS, Goel NK (2010) Fluid-fluid level in pituitary tumors: analysis of management of 106 cases. J Neurosurg 6:1341–1346